sustainability

MDPI

Article

Sensitivity Analysis of Factors Affecting the Bearing Capacity of Suction Bucket Foundation in Soft Clay

Bin Wang [1,2], Ming-Hui Yuan [3], Liang Li [3], Chang-Feng Yuan [3,*], Ying Li [4] and Kan-Min Shen [2]

[1] Key Laboratory of Far-Shore Wind Power Technology of Zhejiang Province, Hangzhou 311122, China
[2] Powerchina Huadong Engineering Corporation Limited, Hangzhou 311122, China
[3] School of Civil Engineering, Qingdao University of Technology, Qingdao 266520, China
[4] Chinese–German Institute of Engineering, Zhejiang University of Science and Technology, Hangzhou 310023, China
* Correspondence: yuanchangfeng@qut.edu.cn; Tel.: +86-131-7323-0827

Abstract: A suction bucket is the foundation for the development of offshore wind power technology in the deep sea, and its stability is crucial to the superstructure of the wind power generation system. Combined with soft clay soil strata along the Chinese coast, the bearing capacity of suction bucket foundations was studied using a numerical model. Sensitivity factors such as soil strength with random space distribution, dimensions of foundation, wind and wave loads in different directions, and cycle times were considered. The results show that the normalized foundation bearing capacity coefficient increases with the increase of the foundation length–diameter ratio. When the foundation length–diameter ratio is less than 1.0, the foundation bearing capacity coefficient is more sensitive to the soil non-uniformity coefficient than the length–diameter ratio. When the length–diameter ratio of the suction bucket is large enough, the influence of the soil non-uniformity coefficient on the bearing capacity of the suction bucket foundation gradually diminishes. When the direction of wind and wave loads is 15°, the bearing capacity of the suction bucket foundation is the weakest. Under the cyclic loads, the shallow soil strength weakens faster in the initial stage and the attenuation rate of soil strength slows down in the latter stage.

Keywords: soft clay; offshore wind power; suction bucket; bearing capacity; sensitivity

Citation: Wang, B.; Yuan, M.-H.; Li, L.; Yuan, C.-F.; Li, Y.; Shen, K.-M. Sensitivity Analysis of Factors Affecting the Bearing Capacity of Suction Bucket Foundation in Soft Clay. *Sustainability* **2022**, *14*, 9615. https://doi.org/10.3390/su14159615

Academic Editors: Jun Hu, Guan Chen and Yong Fu

Received: 24 May 2022
Accepted: 1 August 2022
Published: 4 August 2022

1. Introduction

Offshore wind power has increasingly been a promising alternative to traditional energy. It is one of the most critical issues that the proper selection of foundation type for the construction of offshore wind power. To date, due to the advantages of fast installation and low cost, the monopile foundation [1–3] is one of the most widely used foundations where the water depth is less than 30 m. However, the difficulty and cost of monopile installation will rapidly increase as the depth of the sea increases, which is not conducive to developing deep-sea wind power. Hence, new types of foundations are constantly developed for the deep sea [4,5]. For instance, the multi-pod foundation is suitable for water depths of 30–50 m, but it is difficult to transport and too complicated to install; the jacket foundation is suitable for water depths between 30–60 m, but it has a long manufacturing and installation cycle as well as a high cost that decreases rapidly with the deepening of water depth; the floating foundation is suitable for water depths above 50 m, but it is challenging to design and has the potential to tilt, shake, and overturn. The suction bucket in particular (Figure 1) is a novel deep-sea foundation suitable for water depths above 30 m [6–10]. Compared with the above foundation types, it has the advantages of convenient installation, lower cost, and recyclability.

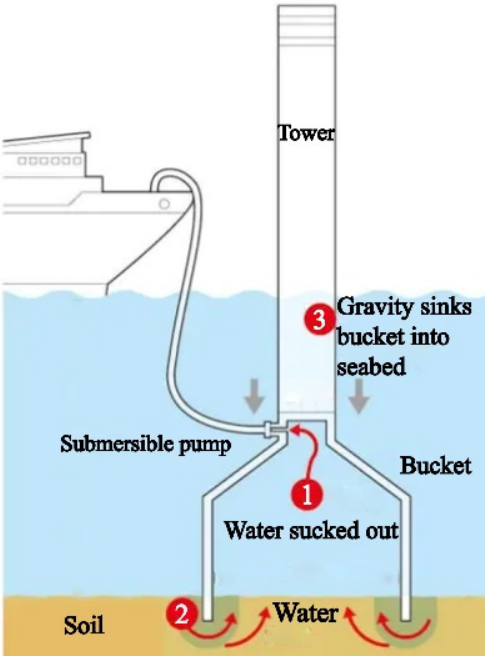

Figure 1. Schematic diagram of suction bucket foundation.

As a new type of foundation for offshore wind power, the suction bucket is primarily a large-diameter barrel with an open bottom and a closed top, which is an alternative form of single pile foundation. The suction bucket has the advantages of low cost, simple construction process, integrated construction, fast installation, and secondary use, which can be better applied to a deep seabed foundation. Meanwhile, the suction bucket foundation [11], which has been effectively developed in recent years, can better resist the large horizontal load and bending moment of wind turbines (Figure 2).

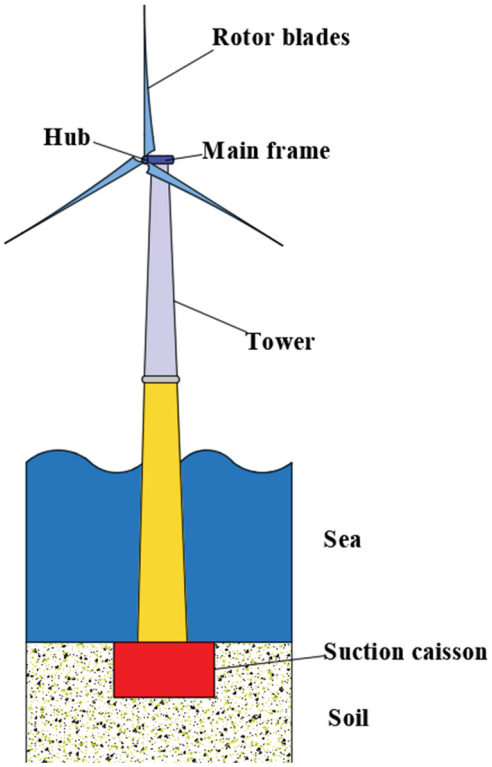

Figure 2. Suction bucket foundation in a wind power generation system.

The study on the bearing capacity characteristics of the suction bucket has attracted much attention. In sand and saturated soft clay, a simple method for estimating the horizontal ultimate bearing capacity of suction bucket foundations has been proposed [12,13]. However, the movement of the foundation rotation center and the complex stress distribution in practical engineering have not been taken into account by this method. Therefore, the calculated bearing capacity was different from the practical engineering. The effect of several swipe loading schemes on the bearing capacity of suction bucket foundations in saturated soft clay and sandy soil has been studied by some scholars. It is worth mentioning that Wu K. and Zhang Y.K.'s results [14,15] are only applicable to foundations in the shallow sea with a small length–diameter ratio. The failure envelope surface of the deep-sea foundations with a large length–diameter ratio needs further study. The limitation of this method is that the actual loads were simplified to the vertical load (V), horizontal load (H), and bending moment (M), which were acted on the midpoint of the top surface of the suction bucket without the horizontal cyclic load. To solve this issue, Wang J.H. [16] studied the effect of vertical loads on the horizontal cyclic bearing capacity of the suction bucket and simulated the suction bucket foundation in soft clay under various vertical and horizontal cyclic loads. According to the results, the vertical load affects the cyclic load amplitude and the number of cycles that lead to the instability and failure of the foundation. The larger the vertical load, the smaller the cyclic load amplitude when the foundation is damaged with the same number of cycles. Therefore, in practical engineering, the vertical load effect caused by various upper fan specifications should be considered and the horizontal bearing capacity should be checked.

According to the Code for Design of Wind Turbine Foundations for Offshore Wind Power Projects (NB/T 10105-2018) [17], the service life of wind turbines should not be less than 25 years. During its 25-year service life, the suction bucket foundation not only bears the long-term effects of its weight and the vertical load transmitted by the superstructure, but also frequently bears the combined effects of horizontal cyclic loads and bending moments caused by wave, ocean currents, wind, etc. When utilized as an offshore wind turbine foundation, it frequently bears larger horizontal loads than vertical loads so that the horizontal load becomes the main controlling load for design. Based on previous engineering experience [18,19], continuous horizontal cyclic loading on the foundation in soft clay will lead to a decrease in soil strength and stiffness, ultimately leading to the destruction of suction bucket foundations before reaching the designed horizontal load. Therefore, it is not entirely reliable to determine the stability of the structure only by relying on the ultimate bearing capacity in the static state. To ensure the accuracy of stability analysis, it is necessary to design a numerical method to accurately predict the ultimate bearing capacity of the suction bucket under horizontal cyclic loads. In this paper, the length–diameter ratio of the suction bucket, soil heterogeneity, the angle between wind and wave loads, and the number of cycles were considered in order to study the bearing characteristics of the suction bucket foundation in saturated soft clay. It is instructive to the analysis of bearing capacity stability in practical engineering.

2. Establishment the Numerical Model

2.1. Overview of the Model

2.1.1. Parameters of the Model

A three-dimensional finite element model of interaction between a single suction bucket and soft clay was established for offshore wind power. The truncated soil model has a radial diameter of 10D (D is the diameter of a suction bucket) and a depth of 6L (L is the length of a suction bucket) [9,14] to ignore boundary effects (Figure 3a). The dimensions of the soil model were verified to be correct by numerical simulation. To improve the computing efficiency, a half model of the bucket–soil system was used for the finite element analysis as the numerical model is symmetrical. The boundary conditions of the soil are as follows: the fixed constraint at the bottom, the lateral radial displacement in the directions of X and Y at the constrained flank of half-cylinder, and the displacement

in the direction of X at the constrained symmetric cross section. A schematic diagram of the model forces is shown in Figure 3b. F_t represents the force transmitted by the superstructure, p represents the pressure difference between the pressure inside the bucket and the atmospheric pressure, $F_{fric\text{-}in}$ and $F_{fric\text{-}out}$ represent the frictional forces generated by the inside and outside of the bucket wall against the soil, and F_Q represents the shear force.

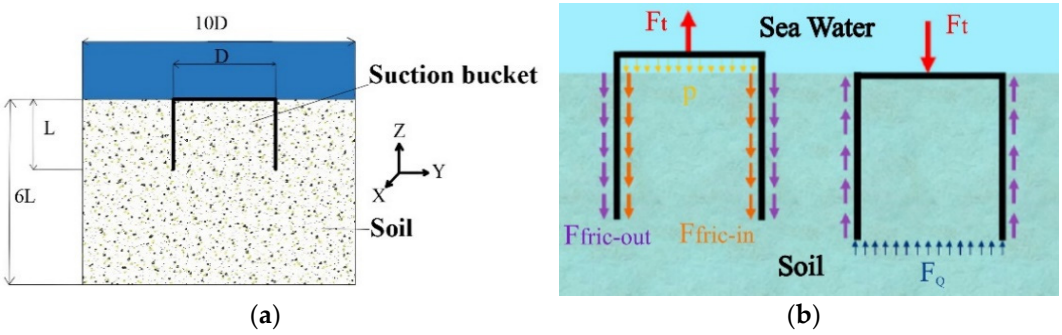

(**a**) (**b**)

Figure 3. The dimensions and forces of the model. (**a**) Dimensions. (**b**) Forces.

The linear elastic constitutive model with elastic modulus was used to simulate the suction bucket, as shown in Table 1. The Mohr–Coulomb elastoplastic constitutive model [13,14,16] is used to simulate the soil, as shown in Table 2. It is assumed that the soil interacts with the suction bucket under completely undrained conditions [2,9,14].

Table 1. Parameters of suction bucket.

Parameters	Elasticity Modulus/GPa	Poisson's Ratio	Effective Weight/(KN·m^{-3})
Bucket	210	0.125	23

Table 2. Parameters of soil.

Parameters	Elasticity Modulus	Poisson's Ratio	Effective Weight/(KN·m^{-3})	Cohesive Force/KPa	Internal Friction Angle/(°)	Dilatancy Angle/(°)
Soil	$500S_u$	0.49	8	20	15	0.1

2.1.2. Mesh

Both the suction bucket and the soil use an integral three-dimensional solid element (C3D8R) with an 8-node hexahedral linear reduction grid (Figure 4). Near the bucket–soil contact surface, cell meshes are densely divided, whereas the mesh is sparse in the soil away from the contact surface [20]. Thus, the calculation time is much shortened and the accuracy of the calculation result is improved.

2.1.3. Interaction between Contact Surfaces

To simulate the shear transfer and relative displacement between the suction bucket and the soil, the contact pairs are defined by the bucket–soil surfaces, including inner, outer, top, and bottom surfaces. The master–slave surfaces contact algorithm is used to choose the master surface. The master surfaces are the surfaces of a suction bucket with high stiffness, and the slave surfaces are the surfaces of soil with low stiffness. The contact pair use face-to-face contact and finite sliding. The tangent behavior of the contact pairs is in the form of a Mohr–Coulomb friction penalty function, and the sliding friction coefficient of the interface is $\mu = \tan(0.75\varphi)$ [21] (φ is the internal friction angle of the soil). The normal behavior of the contact pairs is in the form of hard contact, and the suction bucket and soil can be separated.

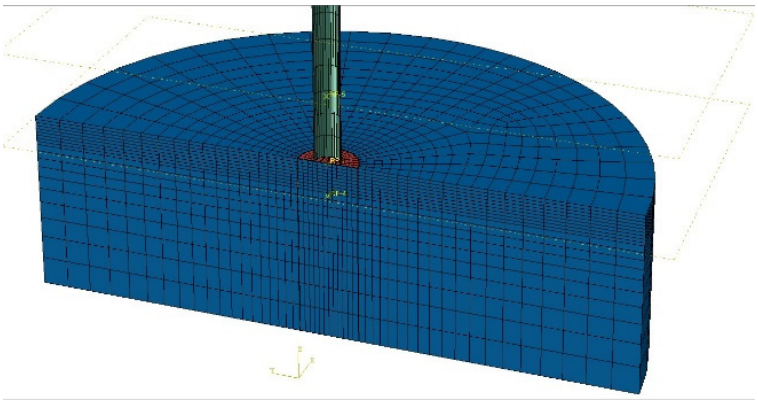

Figure 4. Finite element model.

2.1.4. Initial Geo–Stress Balance

The initial geo–stress was balanced before loading the horizontal cyclic loads by the ODB import method, and the initial geo–stress field was applied to the ground [22]. When the displacement in the direction of Z (U3) reaches 10^{-5}, the additional deformation caused by soil self-gravity is essentially eliminated [23,24].

2.2. Expression of Load

The W3600M-116 offshore wind turbine from China (with 3.6 MW installed capacity) is taken as an example in this paper. H (H = 80 m) is the distance between the hub center and the top surface of the foundation, and G_0 (G_0 = 5200 KN) is the weight of the superstructure transmitted to the foundation. Wind and wave loads are equivalent to horizontal cyclic loads, and cyclic loads are loaded in their respective directions.

Horizontal cyclic loads are defined by periodic amplitude curves in ABAQUS [25]. Fourier series are used to represent periodic amplitude curves.

When $t > t_0$, the amplitude expression is:

$$a = A_0 + \sum_{n=1}^{N} [A_n \cos n\omega(t - t_0) + B_n \sin n\omega(t - t_0)] \quad (1)$$

When $t < t_0$, the amplitude expression is:

$$a = A_0 \quad (2)$$

In Equations (1) and (2), ω is the circular frequency and its value is $\omega = 2\pi f$; f is the frequency; t_0 is the start time; A_0 is the initial amplitude; and A_n is the coefficient of the Cos coefficient and B_n is the Sin coefficient (n = 1, 2, 3 . . . N).

2.3. Determination of Horizontal Cyclic Load

The most dangerous condition, according to most studies, is when the wind and wave loads on the suction bucket foundations are in the same direction. Wind and wave loads are treated as horizontal cyclic loads exerted on the model in this paper (Figure 5). The magnitude, direction, position, and method of loads exerted are all in accordance with the Load Code for the Design of Building Structures (GB50009-2001) [26] and the data of wind and wave loads for an offshore test site in the East China sea. The height of wind load is 80 m over the seabed surface, the frequency is 0.15 Hz, while the height of wave load is 10 m over the seabed surface, the frequency is 0.1 Hz, according to the specifications and practical engineering. The amplitude of wind load is $F_{\text{wind}} = 334000 \sin(0.3\pi t)$, and the amplitude of wave load is $F_{\text{wave}} = 811000 \sin(0.2\pi t)$.

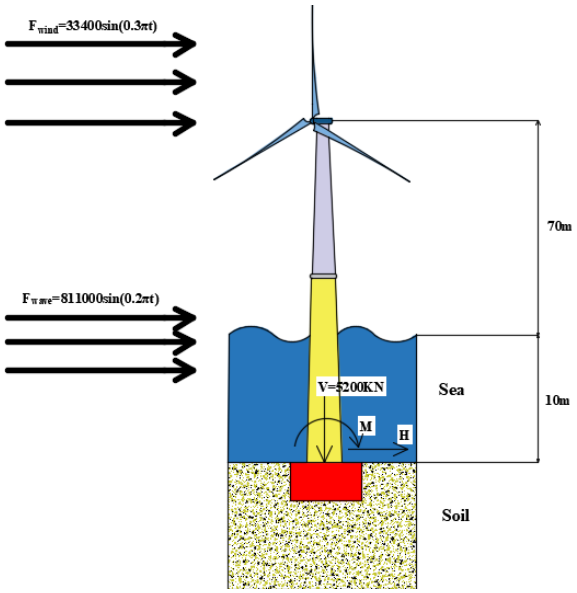

Figure 5. Forces of suction bucket foundation and offshore fan.

2.4. Verification of Finite Element Model

The Equation (3) was used to calculate the relationship between the bearing capacity coefficient and length–diameter ratio (L/D):

$$N_{H,s} = H_{ult,s}/AS_{um} \tag{3}$$

where $N_{H,s}$ is the horizontal ultimate bearing capacity coefficient; $H_{ult,s}$ is the horizontal ultimate bearing capacity; A is sectional area of the suction bucket; and S_{um} is the strength (kPa) of the seabed.

To verify the trustworthiness of the established finite element model, it was compared to existing results [27]. Gelagoti F. et al. set parameters for homogeneous clay, such as L/D = 0.2~1, S_u = 60 kPa, and applied vertical load V = 0 and horizontal force with the method of controlling displacement. In this paper, the same parameters are used, with the exception that the length–diameter ratio (L/D) is increased to 2. When L/D is equal to 1, the calculated results are very close to those found in the literature, with a margin of error of less than 5% (Figure 6). In Figure 6, the horizontal coordinates represent the length-diameter ratio of a suction bucket, and the vertical coordinates represent the horizontal ultimate bearing capacity coefficient.

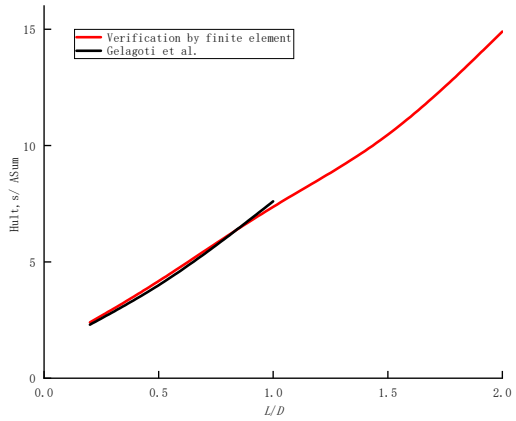

Figure 6. Verification of horizontal bearing capacity coefficients [27].

3. Results

3.1. Bearing Capacity Characteristics with Different Length-Diameter Ratios

The normalized bearing capacity is independent of the diameter of the suction bucket foundation, according to trial calculations and previous studies [28]: suction bucket diameter D = 9 m; suction bucket length L = 4.5, 9, 13.5, and 18 m; length–diameter ratio L/D = 0.5, 1, 1.5, and 2; and suction bucket wall thickness t = 0.1 m.

Assuming that the soil is homogeneous S_{u0} = 5 kPa, the Equation (3) was used to calculate the relationship between the bearing capacity coefficient and length–diameter ratio (L/D). The Figure 7 presents horizontal bearing capacity coefficient with different length–diameter ratios. In Figure 7, the horizontal coordinates represent the length–diameter ratio of a suction bucket, and the vertical coordinates represent the horizontal ultimate bearing capacity coefficient.

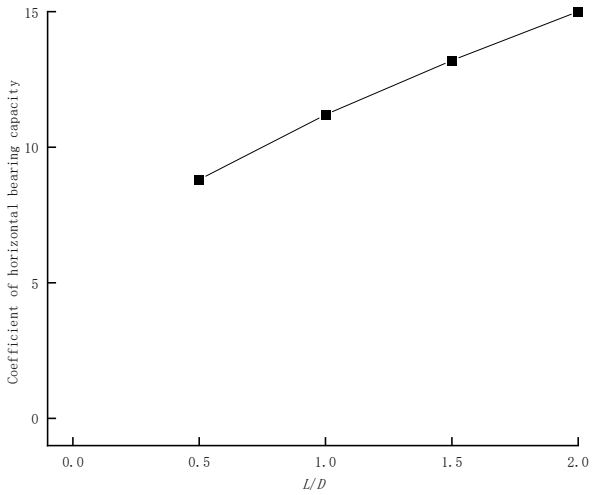

Figure 7. Horizontal bearing capacity coefficient with different L/D.

3.2. Bearing Capacity Characteristics with Different Soil Non-Uniformity Coefficients

Normally consolidated soft clays are widely distributed in the Gulf of Mexico, the South China Sea, and Southeast Asia, and their undrained shear strength S_u increases linearly with depth [29,30], according to Equation (4):

$$S_{um} = KZ + S_{u0} \tag{4}$$

where K is the soil non-uniformity coefficient; Z is the soil depth (m); and S_{u0} is the undrained shear strength of the surface layer. The dimensionless soil non-uniformity coefficient K is used to represent the strength non-uniformity of the soil, according to Equation (5):

$$K = pD/S_{u0} \tag{5}$$

where p is the growth gradient of undrained shear strength along the Z-axis, which is typically 1 to 2.5 kPa/m, p = 1, 1.5, 2, and 2.5 kPa/m are used in this paper; D is the suction bucket diameter (m); and S_{u0} is the undrained shear strength of surface layer.

Five values (K = 0, 1, 2, 5, and 10) are used to investigate the impact of uneven coefficient distribution on bearing capacity characteristics, where K = 0 indicates that the foundation soil is homogeneous soil. The values of K, p, and S_{u0} are shown in Table 3. The horizontal bearing capacity coefficient with different non-uniformity coefficients is presented in Figure 8. In Figure 8, the horizontal coordinates represent the length–diameter ratio of a suction bucket, the vertical coordinates represent the horizontal ultimate bearing capacity coefficient, and the different colored curves represent different soil non-uniformity coefficients.

Table 3. Parameters of K, p, and S_{u0}.

$K = pD/S_{u0}$	p/(kPa·m^{-1})	S_{u0}/kPa
0	0	5
1	1	5
2	1.5	7.5
5	2	4
10	2.5	2.5

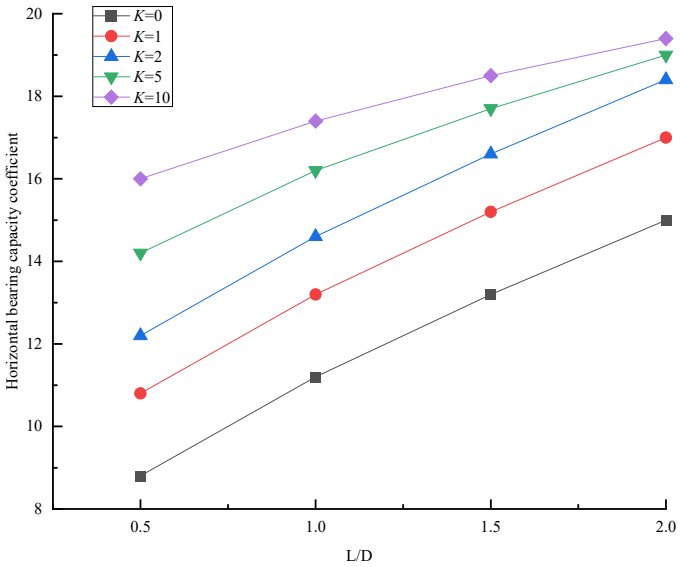

Figure 8. Horizontal bearing capacity coefficient with different non-uniformity coefficients.

3.3. Bearing Capacity Characteristics with Different Angles between Wind and Wave Loads

According to Byrne, B.W., and Houlsby, G.T. [31], the wind and wave load directions are not the same and there is a certain angle between them. According to Seidel [32], the massive horizontal cyclic load induced by wind, wave, and flow does not have a fixed direction, and the included angle of wave load during the service of the offshore fan may exceed 90°. As a result, the wind and wave loads exerted on the offshore fan are not in a single direction, and there is a specific angle θ between them (Figure 9).

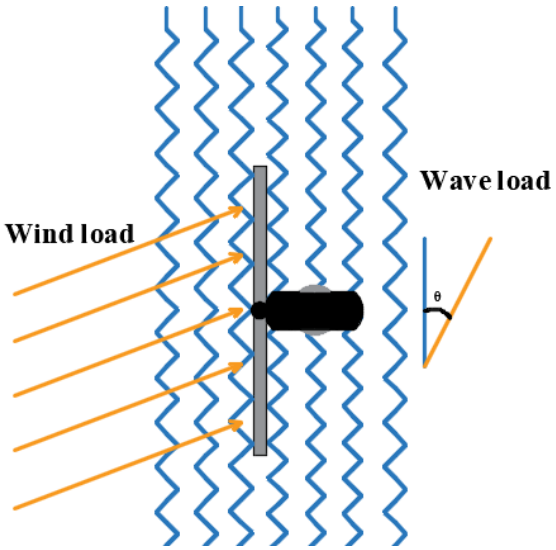

Figure 9. Angles between wind and wave loads.

Generally, the wave load is relatively stable and does not change the direction of action rapidly, whereas turbulent wind causes the wind load to shift the direction rapidly [33]. One-way instability does not occur when the wind and wave loading angle exceeds 45 degrees. As a result, four working conditions of different angles were selected in this paper to investigate the bearing capacity characteristics of the suction bucket. Each working condition is shown in Table 4.

Table 4. Working conditions of wind and wave loading directions.

Working Conditions	Wind Loading Direction	Wave Loading Direction
A	0°	0°
B	0°	15°
C	0°	30°
D	0°	45°

According to the static ultimate bearing capacity and the horizontal displacement corresponding to the ultimate state obtained above, the foundation is judged to have failed when the cyclic displacement amplitude of either of them reaches the ultimate displacement value under the corresponding working condition or if the overall rotation angle of the foundation is 0.05 rad and the corresponding number of cycles when the foundation fails is obtained. The difference in the bearing capacity characteristics of the foundation at different load angles was judged using the number of cycles to failure as an index to compare the bearing characteristics of the foundation. The number of cycles to failure with different wind and wave loading directions is presented in Figure 10. In Figure 10, the horizontal coordinates represent the angle between wind and wave loads, and the vertical coordinates represent the number of cycles in case of foundation failure.

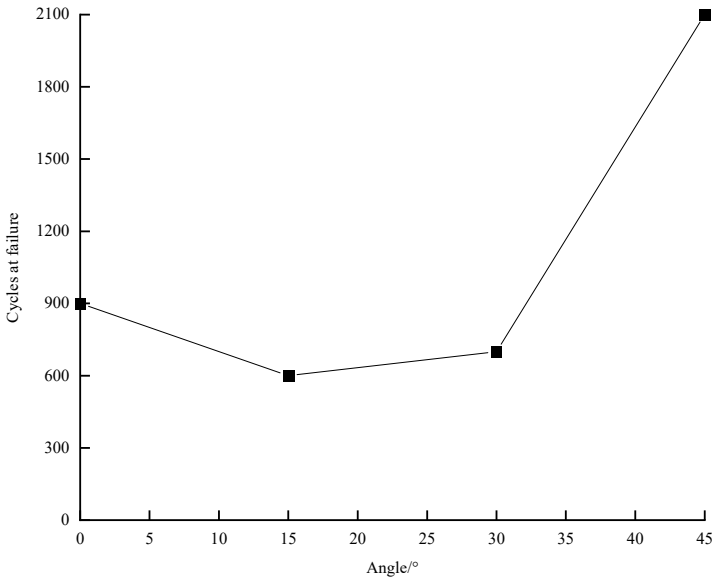

Figure 10. The number of cycles to failure with different wind and wave loading directions.

3.4. Bearing Capacity Characteristics with Different Number of Cycles

Considering the fatigue limit state of the offshore fan foundation and the fact that it will undergo approximately 10 million cyclic loads over the course of a 25-year service life [34], the number of cyclic loads will have a significant impact on the accumulated deformation of the foundation, causing the superstructure to reach the normal limit state ahead of schedule [35]. As a result, it is critical to study the impact of the number of cycles on the foundation. Figure 11 presents the attenuation of horizontal bearing capacity after a different number of cycles. In Figure 11, the horizontal coordinates represent the number

of cycles and the vertical coordinates represent the horizontal bearing capacity. Figure 12 presents the soil strength weakening at different depths. In Figure 12, the horizontal coordinates represent the percentage of the attenuation of bearing capacity after different number of cycles to the bearing capacity in the initial state and the vertical coordinates represent the depth of the soil.

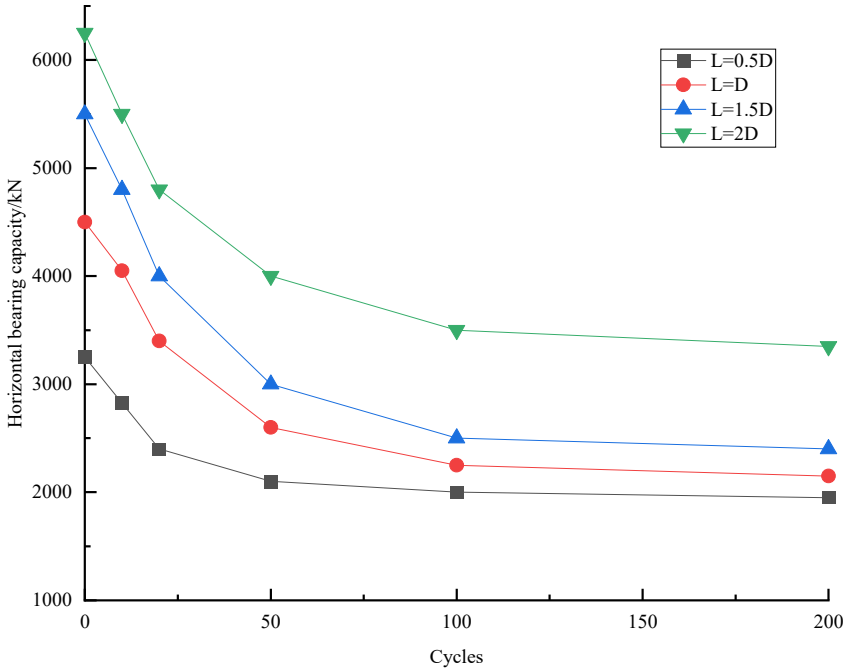

Figure 11. Attenuation of horizontal bearing capacity after different number of cycles.

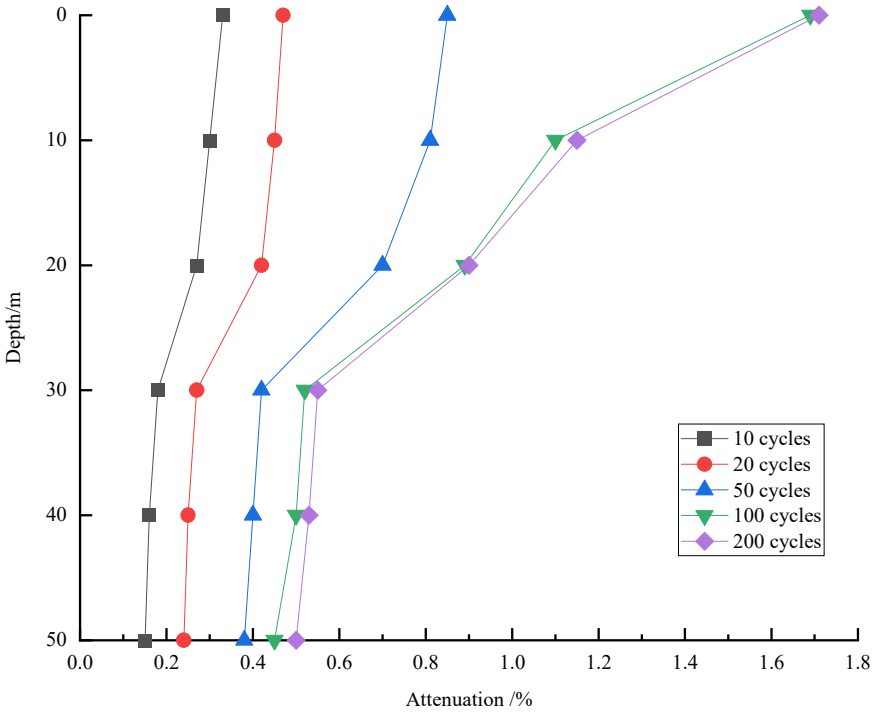

Figure 12. Soil strength weakening at different depths.

4. Discussion

4.1. Sensitivity Analysis of Factor in Length–Diameter Ratios

From the above comparisons of the results from the bearing capacity characteristics with different length–diameter ratios, the horizontal bearing capacity coefficients are respectively calculated while L/D = 0.5, 1.0, 1.5, and 2.0. The horizontal bearing capacity coefficient is 8.8 when L/D = 0.5. The horizontal bearing capacity coefficient increases to 11.2 when L/D is increased to 1.0. The horizontal bearing capacity coefficient increases to 13.2 when L/D is increased to 1.5. The horizontal bearing capacity coefficient increases to 15 when L/D is increased to 2.0. The horizontal bearing capacity coefficient grows constantly as L/D increases, while the rate of increase of bearing capacity drops progressively from 4.8 to 4 and 3.6. When the length–diameter ratio is small, the horizontal bearing capacity coefficient increases with the increase of the length–diameter ratio, but the rate of increase slows down. The bearing capacity coefficient of the suction bucket remains essentially unaltered when the length–diameter ratio is reasonably big and reaches a specific depth. In other words, the buried depth only affects the suction bucket's bearing capacity characteristics within a particular range. The impact is minimal when the threshold is exceeded.

4.2. Sensitivity Analysis of Factor in Soil Non-Uniformity Coefficients

From the above comparisons of the results from the bearing capacity characteristics with different soil non-uniformity coefficients, the horizontal bearing capacity coefficients (K = 0, 1, 2, 5, and 10) are respectively calculated. When the length–diameter ratio is 0.5, the horizontal bearing capacity coefficients (K = 0, 1, 2, 5, and 10) are 8.8, 10.8, 12.2, 14.2, and 16 respectively. It indicates that the horizontal bearing capacity coefficient increases as the non-uniformity coefficient K increases. When the length–diameter ratio is 2.0, the horizontal bearing capacity coefficients (K = 0, 1, 2, 5, 10) are 17, 18.4, 19, 19.4, respectively. It verifies that the influence of soil unevenness coefficient on the bearing capacity coefficients is greater than the influence of the length–diameter ratio when the length–diameter ratio is small, while the length–diameter ratio is large enough, the influence of soil non-uniformity coefficient on the bearing capacity of the suction bucket foundation gradually diminishes.

4.3. Sensitivity Analysis of Factor in Angles between Wind and Wave Loads

From the above comparisons of the results from the bearing capacity characteristics with different angles between wind and wave loads, when the wind and wave loading angle is 15° to 30°, the bearing capacity characteristic of the foundation is weakened to some extent compared to the loading direction collinearity. The reason for this is that the type of load exerted on the foundation varies. Although the value is minor, the wind load causes a substantial bending moment in the foundation, making the bearing characteristics in the direction of about 15° to 30° weaker than in the direction of 0°. Furthermore, the lateral displacement of the wave load promotes the foundation's instability. The results show that a particular load angle causes the foundation's bearing capacity to deteriorate, putting the suction bucket foundation in jeopardy.

4.4. Sensitivity Analysis of Factor in Number of Cycles

As can be seen from the above comparisons of the results and from the bearing capacity characteristics with different number of cycles, the horizontal bearing capacity of a suction bucket foundation initially decreases rapidly as the number of cycles increases. The horizontal bearing capacity had decreased by more than 95% after 100 cycles. The weakening of soil strength is related to the attenuation of horizontal bearing capacity after cyclic loading. The plastic strain will appear after the soil has been subjected to cyclic load. The accumulation of plastic strain leads to soil strength weakening, and the degree of soil strength weakening decreases gradually as plastic strain accumulates.

The soil stress at different depths decreases with the increase in the number of cycles after the suction bucket is subjected to the horizontal cyclic load, and the shallow soil stress

decreases much more than deep soil. After about 100 cycles, the soil stress at shallow gradually increases and is basically stable, whereas the soil stress at deep continues to decrease but the amplitude becomes low. As a result, when a suction bucket is subjected to cyclic loading, the strength of shallow soil deteriorates rapidly because it serves as the primary source of horizontal bearing capacity, whereas the strength of deep soil deteriorates slowly. The strength of deep soil causes attenuation even when the horizontal bearing capacity is essentially stable.

5. Conclusions

A numerical model of the interaction between the suction bucket and saturated soft clay was established. The sensitivity of different factors affecting the bearing capacity of the suction bucket foundation, including length–diameter ratios, soil heterogeneity, angles between wind and wave loads, and the number of cycles was analyzed. Based on the above results and discussion, the following conclusions can be drawn:

1. The relationship between the horizontal bearing capacity coefficient and the length-diameter ratio and the soil unevenness coefficient has been established through numerical simulation, and the results show that the length–diameter ratio and the unevenness coefficient are positively correlated to the horizontal bearing capacity coefficient.
2. When the length–diameter ratio of suction bucket is less than 1.0, the influence of the soil non-uniformity coefficient on the bearing capacity of the suction bucket foundation is greater than length–diameter ratio.
3. When the length–diameter ratio of the suction bucket is more than 2.0, the influence of soil non-uniformity coefficient on the bearing capacity of the suction bucket foundation gradually diminishes.
4. When the angle between wind and wave loads is 15° to 30°, the bearing capacity of the suction bucket foundation is lower than the bearing capacity when the wind and wave loads are collinear.
5. The attenuation of soil strength is rapid within 60 cycles. Because the shallow soil layer is the primary provider of horizontal bearing capacity during the initial cycles, the rate of strength attenuation in the shallow soil is faster than that in the deep soil under initial cyclic loads.
6. The attenuation of soil strength is slow after 100 cycles. Because the strength of shallow soil is relatively stable after 100 cycles, the reason for the subsequent slow strength attenuation is that the strength of deep soil decreases.

Author Contributions: Conceptualization, B.W. and C.-F.Y.; methodology, L.L.; software, M.-H.Y.; validation, M.-H.Y. and C.-F.Y.; formal analysis, L.L.; data curation, Y.L.; writing—original draft preparation, B.W. and M.-H.Y.; writing—review and editing, C.-F.Y. and L.L.; visualization, K.-M.S.; funding acquisition, B.W. All authors have read and agreed to the published version of the manuscript.

Funding: This research was funded by the National Natural Science Foundation of China (Grant No. 51909238, 51939002, 52101334, 52071301), the Open Fund of Zhejiang Provincial Key Laboratory of Deep-sea Wind Power Technology Research (Grant No. ZOE2020006) and Zhejiang Provincial Natural Science Foundation of China (LHY21E090001).

Institutional Review Board Statement: Not applicable.

Informed Consent Statement: Not applicable.

Data Availability Statement: Not applicable.

Acknowledgments: The authors would like to acknowledge the funding for support. Finally, we would also like to thank the associate editor of this Special Edition, and the reviewers who provided constructive feedback that has without doubt improved this manuscript.

Conflicts of Interest: Authors B.W. and K.-M.S. are employed by Powerchina Huadong Engineering Corporation Limited. The remaining authors declare that the research was conducted in the absence of any commercial or financial relationships that could be construed as a potential conflict of interest.

References

1. Zou, L.; Tang, H.Y.; Wang, Y.H.; Chen, P.; Huang, X.G.; Wu, W. Development of Foundation Structure Selection Program of Offshore Wind Turbines. *Ship Eng.* **2020**, *42*, 282–285. (In Chinese)
2. Sun, Y.X. Experimental and Numerical Studies on a Laterally Loaded Monopile Foundation of Offshore Wind Turbine. Ph.D. Thesis, Zhejiang University, Zhejiang, China, 2016. (In Chinese).
3. Xie, M.; Lopez-Querol, S. Numerical Simulations of the Monotonic and Cyclic Behavior of Offshore Wind Turbine Monopile Foundations in Clayey Soils. *J. Mar. Sci. Eng.* **2021**, *9*, 1036. [CrossRef]
4. Amin, B.; Britta, B.; Domenico, L.; Shinji, S. Offshore Wind Turbine Foundations. *Soils Found.* **2021**, *61*, 621–622.
5. Li, J.W.; Hu, G.Q.; Jin, G.Q. Hydrodynamic Performance of a Novel Floating Foundation for an Offshore Wind Turbine Under a Storm Condition. *Int. J. Offshore Polar Eng.* **2020**, *30*, 120–128. [CrossRef]
6. Tjelta, T.L. Geotechnical Aspects of Bucket Foundations Replacing Piles for the Europipe 16/11-E Jacket. In Proceedings of the Offshore Technology Conference, Houston, TX, USA, 2 May 1994.
7. Shi, X.C.; Xu, R.Q.; Gong, X.N.; Chen, G.X.; Yuan, Z.L. Introduction of Bucket Foundation. *Chin. Civil Eng. J.* **2000**, *33*, 68–92. (In Chinese)
8. Yang, J.L.; Wang, S.F.; Kong, L.W.; Yuan, J.X.; Liu, Z.A.; Wang, Q. The 3-D Finite Element Analysis of Stability of Platform with Bucket Foundation. *Rock Soil Mech.* **2002**, *23*, 640–644. (In Chinese)
9. Wu, K.; Xue, H.F.; Chen, R.; Li, S.C. Studies on Bearing Capacity of Composite Multi-Suction Bucket Structure of Suctional Suction Bucket Foundation. *J. Disaster Prev. Mitigation Eng.* **2008**, *28*, 484–491. (In Chinese)
10. Li, D.Y.; Chen, Q.J.; Zhang, Y.K.; Chen, F.Q. Review of Horizontal Loading on Suction Caisson of Offshore Wind Turbines. *Ocean Eng.* **2020**, *38*, 137–147. (In Chinese)
11. Wu, X.N.; Liao, Q.; Li, Y. A Review on the Bearing Capacity Studies of the Suction Bucket Foundation for Offshore Wind Turbines. *J. Ocean Technol.* **2020**, *39*, 91–106. (In Chinese)
12. Jin, S.C.; Zhang, Y.T.; Yang, Y.H.; Li, B. Research on Horizontal Ultimate Bearing Capacity of Suction Bucket Foundation in Saturated Sand Ground in Saturated Sand Ground. *Rock Soil Mech.* **2013**, *34*, 221–227. (In Chinese)
13. Sun, X.Y.; Luan, M.T.; Tang, X.W. Study of Horizontal Bearing Capacity of Bucket Foundation on Saturated Soft Clay Ground. *Rock Soil Mech.* **2010**, *31*, 667–672. (In Chinese)
14. Wu, K.; Luan, M.T.; Fan, Q.L.; Wang, Z.Y. Numerical Analysis of Failure Envelopes of Bucket Foundation Subjected to Combined Loads Based on Elasto-plastic Fem. *Eng. Mech.* **2008**, *25*, 156–161. (In Chinese)
15. Zhang, Y.K.; Wang, C.C.; Li, D.Y.; Qi, Y.S. Numerical Simulation of Bearing Characteristics of Modified Suction Cassions in Sand Under Combined Loads. *Sci. Technol. Eng.* **2021**, *21*, 1515–1521. (In Chinese)
16. Wang, J.H.; Yang, H.M. Model test on Horizontal Cyclic Bearing Capacity of Bucket Foundations in Soft Clays. *Rock Soil Mech.* **2008**, *29*, 2606–2612. (In Chinese)
17. Zhao, S.X.; Sun, B.B. *Code for Design of Wind Turbine Foundations for Offshore Wind Power Projects (NB/T 10105-2018)*, 1st ed.; Yi, Y.C., Xie, H.W., Eds.; China Water & Power Press: Beijing, China, 2019; pp. 3–4.
18. Hong, Z.B.; Tao, J.G.; Hu, D.; Li, F.; Xie, X.T. Research on the Stiffness Degradation Model of Saturated Soft Clay Seabed under Cyclic Loading. *J. Railw. Sci. Eng.* **2021**, *18*, 351–358. (In Chinese)
19. Fan, Q.L. A Study on Stability of Deeply-Embedded Large-Diameter Cylindrical Structure in Soft Ground. Ph.D. Thesis, Dalian University of Technology, Liaoning, China, 2007. (In Chinese).
20. Chen, G.; Beer, M.; Liu, Y. Modeling Response Spectrum Compatible Pulse-like Ground Motion. *Mech. Syst. Signal Proc.* **2022**, *177*, 109177. [CrossRef]
21. Liu, J.C.; Xiong, G.; Zhu, B.; Ying, P.P. Bearing Capacity and Deflection Behaviors of Large Diameter Monopile Foundations in Sand Seabed. *Rock Soil Mech.* **2015**, *36*, 591–599. (In Chinese)
22. Liu, Y.; Jiang, Y.; Xiao, H.; Lee, F.H. Determination of Representative Strength of Deep Cement-Mixed Clay from Core Strength Data. *Géotechnique* **2017**, *67*, 350–364. [CrossRef]
23. Liu, Y.; Lee, F.H.; Quek, S.T.; Chen, E.J.; Yi, J.T. Effect of Spatial Variation of Strength and Modulus on the Lateral Compression Response of Cement-Admixed Clay Slab. *Géotechnique* **2015**, *65*, 851–865. [CrossRef]
24. Wang, R.H.; Li, D.Q.; Chen, E.J.; Liu, Y. Dynamic Prediction of Mechanized Shield Tunneling Performance. *Autom. Constr.* **2021**, *132*, 103958. [CrossRef]
25. Cao, J.F.; Shi, Y.P. *Answers to Common Issues of Finite Element Analysis in ABAQUS*, 1st ed.; Kong, J., Guo, J., Eds.; China Machine Press: Beijing, China, 2009; pp. 109–114.
26. Jin, X.Y.; Wang, J. *Load Code for the Design of Building Structures (GB50009-2012)*, 1st ed.; Chen, M.K., Wang, D.S., Eds.; China Architecture Publishing & Media Co., Ltd.: Beijing, China, 2012; pp. 30–62.
27. Gelagoti, F.; Georgiou, I.; Kourkoulis, R.; Gazetas, G. Nonlinear Lateral Stiffness and Bearing Capacity of Suction Caissons for Offshore Wind-Turbines. *Ocean Eng.* **2018**, *170*, 445–465. [CrossRef]
28. Zhou, S.J.; Zhang, Y.; Wang, D. Capacity Envelope of Caisson Foundation for on-bottom Pipelines. *Mar. Sci. Bull.* **2019**, *38*, 727–732. (In Chinese)
29. Chen, X.J.; Li, D.Q.; Tang, X.S.; Liu, Y. A Three-Dimensional Large-Deformation Random Finite-Element Study of Landslide Runout Considering Spatially Varying Soil. *Landslides* **2021**, *18*, 3149–3162. [CrossRef]

30. Liu, Y.; He, L.Q.; Jiang, Y.J.; Sun, M.M.; Chen, E.J.; Lee, F.H. Effect of in-Situ Water Content Variation on the Spatial Variation of Strength of Deep Cement-Mixed Clay. *Géotechnique* **2019**, *69*, 391–405. [CrossRef]
31. Byrne, B.W.; Houlsby, G.T. Foundations for Offshore Wind Turbines. *Philos. Trans. R. Soc. Lond. Ser. A* **2003**, *361*, 2909–2930. [CrossRef]
32. Seidel, M. Feasibility of Monopiles for Large Offshore Wind Turbines. In Proceedings of the 10th German Wind Energy Conference (DEWEK), Bremen, Germany, 17–18 November 2010.
33. Fischer, T.; Rainey, P.; Bossanyi, E.; Kühn, M. Study on Control Concepts Suitable for Mitigation of Loads from Misaligned Wind and Waves on Offshore Wind Turbines Supported on Monopiles. *Wind Eng.* **2011**, *35*, 561–574. [CrossRef]
34. Schaumann, P.; Lochte-Holtgreven, S.; Steppeler, S. Special Fatigue Aspects of Support Structures with Offshore Wind Turbines. *Materialwiss. Werkstofftech.* **2011**, *42*, 1075–1081. [CrossRef]
35. Liu, Y.; Li, K.Q.; Li, D.Q.; Tang, X.S.; Gu, S.X. Coupled Thermal–Hydraulic Modeling of Artificial Ground Freezing with Uncertainties in Pipe Inclination and Thermal Conductivity. *Acta Geotech.* **2022**, *17*, 257–274. [CrossRef]